THE JOURNAL OF PHYSICAL CHEMISTRY C
A JOURNAL OF THE AMERICAN CHEMICAL SOCIETY

pubs.acs.org/JPCC

Article

Promoted Thermal Reduction of Copper Oxide Surfaces by N-Heterocyclic Carbenes

Published as part of The Journal of Physical Chemistry virtual special issue "Cynthia Friend Festschrift".

Juan J. Navarro, Mowpriya Das, Sergio Tosoni,* Felix Landwehr, Markus Heyde,* Gianfranco Pacchioni, Frank Glorius,* and Beatriz Roldan Cuenya

Cite This: *J. Phys. Chem. C* 2022, 126, 17528−17535

Read Online

ACCESS | Metrics & More | Article Recommendations | Supporting Information

ABSTRACT: The influence of metallic and oxide phases coexisting on surfaces is of fundamental importance in heterogeneous catalysis. Many reactions lead to the reduction of the oxidized areas, but the elucidation of the mechanisms driving these processes is often challenging. In addition, intermediate species or designed organic ligands increase the complexity of the surface. In the present study, we address the thermal reduction of a copper oxide overlayer grown on Cu(111) in the presence of N-heterocyclic carbene (NHC) ligands by means of scanning tunneling microscopy (STM) and density functional theory (DFT). We show that the NHC ligands actively participate in the copper oxide reduction, promoting its removal at temperatures as low as 470 K. The reduction of the oxide was tracked by employing scanning tunneling spectroscopy (STS), providing a chemical identification of metallic and oxide areas at the nanometric scale.

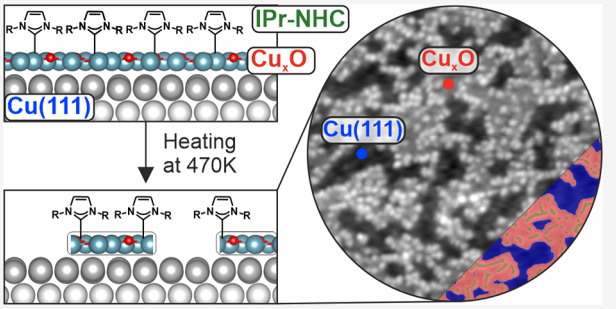

INTRODUCTION

The interplay between metallic and oxide phases is key in many catalytic reactions.[1] This fact is especially important in reactions involving copper catalysts such as CO_2 electroreduction,[2] CO oxidation,[3] or water−gas shift.[4,5] Since the interaction with intermediate species or added ligands strongly influences the reaction pathways, it is necessary to understand how molecular species react with the different copper phases[6] and what mechanisms lead to the reduction of the copper oxide areas. In addition, the design of the ligands for the modification of the surfaces represents a chance to tune the catalytic processes.[7,8]

N-Heterocyclic carbenes (NHCs)[9] have opened new avenues in the functionalization of metal surfaces, providing strong ligand−metal bonds that allow for interesting applications in various fields.[10−16] The use of NHC species in heterogeneous catalysis[17−23] also includes their attachment to copper catalysts, for example, in semihydrogenation processes or in the hydrogen evolution reaction.[24,25] However, a fundamental understanding of the interaction of these ligands with metal surfaces prone to oxidation, like copper, is still limited.[26−30]

The deposition of NHC on copper oxide in solution was reported by Veinot et al.,[27] resulting in the spontaneous reduction of the oxide layer at room temperature and subsequent attachment of the ligands on the metallic copper surface. In this study, copper oxide species were still present after the attachment of the NHC ligands. The sample preparation under ultrahigh vacuum (UHV) conditions allows for a better control of the surface structure and the chemical composition than in solution. In an UHV, it has been reported that a copper oxide overlayer stays on the Cu(111) surface even after annealing at 770 K.[31] Other thin film studies reported the presence of copper oxide at temperatures as high as 1070 K.[32,33] Herein, we show that the thermal reduction of a oxidized copper surface under UHV conditions requires considerably lower temperatures in the presence of a model NHC (1,3-bis(2,6-diisopropylphenyl)imidazol-2-ylidene, IPr-NHC). The removal of the oxide areas is locally investigated by means of scanning tunneling microscopy (STM) and scanning tunneling spectroscopy (STS). X-ray photoelectron spectroscopy (XPS) and density functional theory (DFT) provide further insight into the reduction process.

EXPERIMENTAL METHODS

As a precursor for IPr-NHC, we used bench-stable 1,3-bis(2,6-diisopropylphenyl)-1*H*-imidazol-3-ium-2-carboxylate (IPr-CO_2

Received: June 20, 2022
Revised: September 21, 2022
Published: October 6, 2022

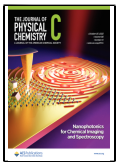

adduct), which is known to generate free IPr-NHC under heating in an ultrahigh vacuum with only gaseous CO_2 as a byproduct. This enables a very clean NHC deposition on the surface without any further impurities (Scheme 1). For the synthesis of the IPr-CO_2 adduct, a modified procedure from the literature was followed (see the Supporting Information).[34,35]

Scheme 1. Deposition of IPr-NHC on Cu_xO/Cu(111)[a]

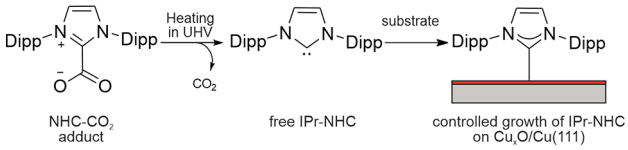

[a]Heating of the IPr-CO_2 precursor at 340 K under an UHV in a Knudsen cell leads to a molecular flux of free IPr-NHC. The adsorption takes place by exposing the surface to the molecular flux. Dipp: 2,6-diisopropylphenyl.

The Cu(111) surface was prepared by combining sputtering with Ar^+ at 1 kV for 30 min and annealing at 950 K for 5 min in a UHV chamber with a base pressure of $\lesssim 5\times 10^{-10}$ mbar. A Cu_xO layer was grown by exposing the copper substrate at 670 K to an oxygen partial pressure of 5×10^{-7} mbar and subsequent annealing in an UHV at 720 K. IPr-NHC molecules were evaporated by resistive heating in a Knudsen cell at 340 K, leading to a deposition rate of 0.05 monolayers/min on the bare Cu(111) surface. The molecules were deposited by keeping the Cu substrate at 310 K. STM images were taken in constant current mode at 5 K using a PtIr tip. STS data were acquired at 5 K in a constant current mode and an active feedback loop employing an external lock-in amplifier with a modulation signal of 80 mV. XPS data were obtained at room temperature using an Al anode operating at 300 W as the X-ray source and a Phoibos 100 analyzer.

COMPUTATIONAL METHODS

All calculations were done with the code VASP.[36,37] The core electrons were modeled with the Projector Augmented Wave (PAW) method,[38,39] while H(1s), C(2s,2p), N(2s,2p), O-(2s,2p), and Cu(3d,4s) electrons were treated explicitly with a set of plane waves expanded up to a kinetic energy cutoff of 400 eV. The PBE exchange-correlation functional[40] was adopted, including the long-range dispersion according to the DFT+D2′ scheme.[41,42] Structure relaxations were performed with thresholds of 10^{-5} eV and 10^{-2} eV/Å for electronic and ionic loops, respectively. The sampling in the reciprocal space was reduced to the Γ point due to the large dimension of the supercells. The dipole correction was applied along the nonperiodic direction and an empty layer of at least 15 Å thickness was included in every supercell. The Cu lattice constant was at first relaxed, yielding 3.57 Å. The Cu(111) surface was then simulated by a five-layer slab, where the ionic coordinates of the three topmost layers were relaxed, while the ions from the two bottom layers were frozen in their bulk positions. A cuprite (111) single layer with periodicity ($\sqrt{7} \times \sqrt{7}$ R19°) was then added on top of a 7 × 7 Cu(111) supercell (17.67 Å × 17.67 Å) with a reciprocal rotation of 11°. Such a coincidence lattice ensures a good match between the cuprite overlayer and the support as well as enough space to simulate the adsorption of the ligand in various configurations (vide infra). This model, albeit simplified, displays a hexagonal ring motif common to more sophisticated structures proposed for the Cu_xO "29" phase.[43] Its formation energy with respect to its unbound components (clean Cu(111), pure metallic Cu, and a gas-phase O_2 molecule) is −1.8 eV per O atom, a value comparable to those reported by Therrien et al. for their most stable structures.[43] Adsorption of a single IPr-NHC was then simulated on this supercell, allowing relaxation of the molecule as well as the substrate (beside the two bottom Cu layers). The adsorption energy, D_e, is defined as the energy of the molecule/substrate adduct with respect to the energy of its

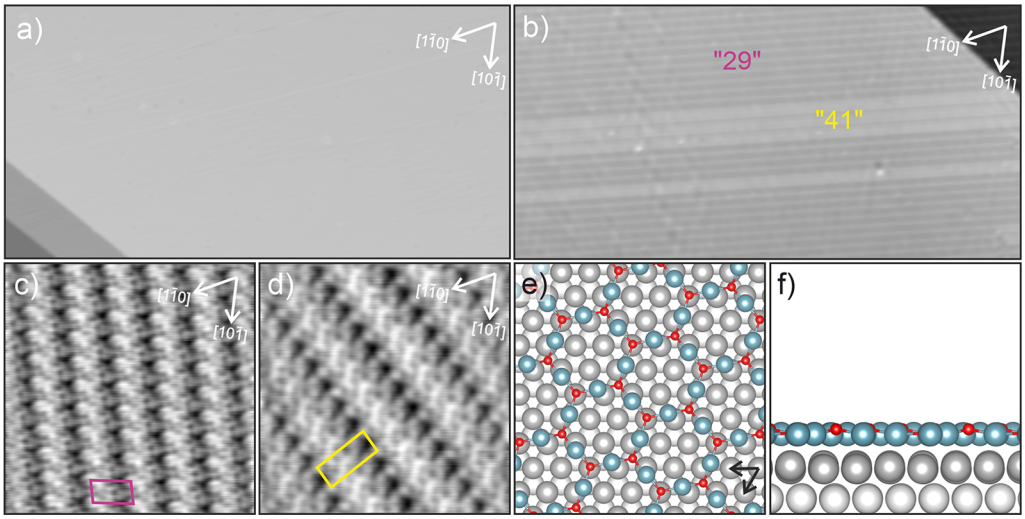

Figure 1. STM images for the differently prepared surfaces acquired at 5 K. (a) Cu(111): 100 nm × 50 nm, V_s = 0.5 V, I_t = 300 pA; (b) Cu_xO overlayer on Cu(111): 100 nm × 50 nm, V_s = 0.8 V, I_t = 20 pA; (c) "29" Cu_xO structure, 10 nm × 10 nm, V_s = −0.2 V, I_t = 50 pA; (d) "41" Cu_xO structure, 10 nm × 10 nm, V_s = −0.2 V, I_t = 50 pA. Unit cells of the oxide structures are marked by red and yellow parallelograms. (e, f) Top and side view of a Cu_2O(111) layer on Cu(111). Unit cell vectors of Cu(111) are indicated (black arrows). In the STM images, white arrows indicate the high symmetry directions of Cu(111).

https://doi.org/10.1021/acs.jpcc.2c04257
J. Phys. Chem. C 2022, 126, 17528−17535

separated components, where negative values imply stable bonding:

$$D_e = E(\mathrm{IPrNHC/Cu_xO/Cu}) - [E(\mathrm{IPrNHC}) + E(\mathrm{Cu_xO/Cu})] \quad (1)$$

RESULTS AND DISCUSSION

As a starting point, the bare Cu(111) surface was prepared to check the cleanness and size of the terraces by STM, leading to images like that in Figure 1a. After the thermal oxidation of the surface, a thin layer showing row-like structures, characteristic for Cu_xO overlayers, appears (Figure 1b). The rows extend across regions larger than 300 nm without being distorted by the steps. This fact may indicate that, at some point after the thermal oxidation process, copper atoms from the Cu(111) surface still diffuse underneath the oxide overlayer before forming the terraces. Two coexisting Cu_xO phases can be distinguished. The most abundant phase corresponds to the widely studied "29" Cu_xO structure,[31,43−45] whose unit cell is marked in the atomically resolved image of Figure 1c and corresponds to a $\sqrt{13}$ R46.1° × 7 R21.8° superlattice.[45] Interestingly, we found an additional phase that extends in the same direction as the "29" structure and matches the recently reported "41" structure (Figure 1d).[46] The "44" structure was not observed under the conditions reported in the present study. These large unit cells can be interpreted as substructures emerging from a $Cu_2O(111)$ layer that are commensurate with respect to the Cu(111) surface.[45] In addition, the resulting copper oxide layer is considered to be two-dimensional.[47] The computational modeling in this paper relies on a simplified model of a nondistorted $Cu_2O(111)$ layer shown in Figure 1e,f, as discussed before.[48]

The arrangement of IPr-NHC ligands on the bare Cu(111) surface results in a hexagonal molecular lattice forming well-defined structures, as reported recently by the authors.[30] For example, after the molecules were deposited for 5 min on Cu(111), molecular islands appear, as shown in Figure 2a. The deposition of IPr-NHC on the Cu_xO layer under the same evaporation conditions leads to a very different arrangement (Figure 2b). Instead of forming closed-packed islands, the molecules are distributed over the whole surface, often individually attaching on the Cu_xO, and arranged in a row pattern. In addition, the coverage is slightly higher as compared to that of the bare surface, which indicates an increase in reactivity. A higher coverage of IPr-NHC on Cu_xO/Cu(111) (10 min deposition) leads to a clearer row pattern (Figure 3a,b). Interestingly, the distance between rows, ca. 1.7 nm, is very close to the length of one of the lattice vectors of the abundant "29"-Cu_xO structure. The rest of the molecules, arranged differently, probably occupy areas of the "41"-Cu_xO structure. The lower degree of order observed in these areas could be related to the larger unit cell of the "41" phase,[46]

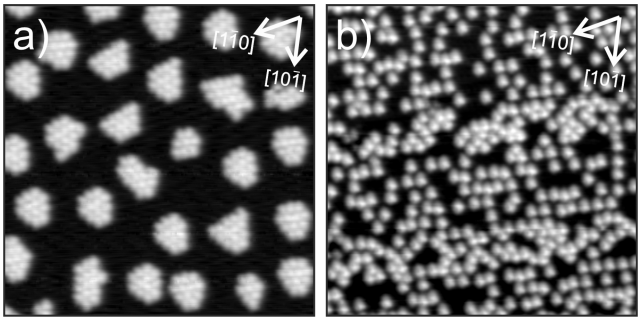

Figure 2. IPr-NHC on bare Cu(111) and on Cu_xO/Cu(111). (a) Bare Cu(111), 40 nm × 40 nm, V_s = 1.5 V, I_t = 20 pA; (b) Cu_xO/Cu(111), 40 nm × 40 nm, V_s = 1.0 V, I_t = 80 pA. IPr-NHC deposited for 5 min on both substrates under the conditions reported in the Experimental Methods section. High symmetry directions of Cu(111) are indicated (white arrows).

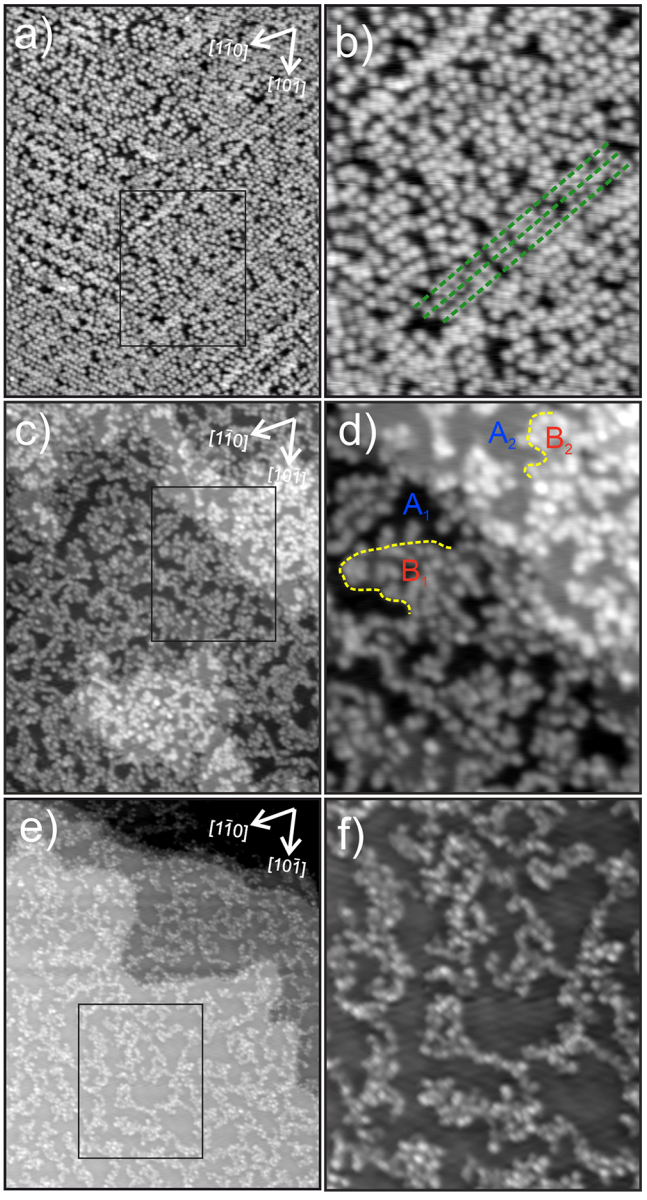

Figure 3. STM images showing the surface after consecutive annealing steps. (a) As-prepared IPr-NHC on Cu_xO/Cu(111), 100 nm × 124 nm, V_s = 1.0 V, I_t = 20 pA. (b) Magnified STM image from the black square in (a), 40 nm × 50 nm. Green dotted lines indicate the orientation of the molecular rows. (c) After 470 K annealing, 100 nm × 124 nm, V_s = 1.0 V, I_t = 20 pA. (d) Magnified STM image from the black square in (c), 40 nm × 50 nm. A (A_1 and A_2) and B (B_1 and B_2) areas are labeled. The edges between them are marked by a yellow dotted line. (e) After 520 K annealing, 100 nm × 124 nm, V_s = 1.0 V, I_t = 20 pA. (f) Magnified STM image from the black square in (e), 40 nm × 50 nm. High symmetry directions of Cu(111) marked by white arrows.

https://doi.org/10.1021/acs.jpcc.2c04257
J. Phys. Chem. C 2022, 126, 17528−17535

compared to the "29" structure, which may lead to a weaker confinement of the molecules. These data suggest a remarkable influence of the underlying oxide support structure on the molecular arrangement and thus a strong interaction between the IPr-NHC ligands and the Cu_xO overlayer. Furthermore, in previous publications, the authors show that IPr-NHC ligands can bind covalently to the $Cu_xO/Cu(111)$ surface.[49] The resulting NHC assemblies are stable at temperatures up to 420 K, as shown in Figure S1.

In order to assess the thermal stability of the surface, we heated the sample to 470 K for 1 min. This treatment leads to drastic structural changes (Figure 3c). The structures found in the as-prepared sample disappear, giving rise to a quite complex surface. Although some molecules are difficult to identify, we estimate that 43 ± 6% of them desorbed during the annealing step. Two different areas, marked in Figure 3d, can be distinguished. One type of area, A, is mostly unoccupied by the ligands, while the other area, B, seems to be a favorable region for the adsorption of IPr-NHC molecules. In particular, the edges of the B areas present a high amount of adsorbed molecules. Therefore, A and B areas present very different reactivity. At the tunneling conditions of Figure 3c, the apparent height for the steps between the A and B regions reaches a value of ca. 0.1 nm (Figure S2), which is well below the apparent height for the Cu(111) steps (0.21 nm). On the other hand, this value for the Cu(111) steps matches the apparent height between the A areas (for example, A_1 and A_2 regions shown in Figure 3d).

Annealing the surface to 520 K for 1 min results in further changes. As can be seen in Figure 3e,f, the A and B regions do not appear anymore, while the terraces exhibit disordered aggregates with a broad range of apparent heights (Figure S2). These aggregates are probably remaining species produced during on-surface reactions taking place between the NHC ligands and the Cu_xO layer during annealing. They form an extended network across the surface, not allowing the identification of single IPr-NHC ligands.

Scanning tunneling spectroscopy (STS) can be very useful for getting chemical information of the surface. In particular, Cu(111) and Cu_xO surfaces exhibit characteristic field emission resonances (FERs) in the dI/dV spectra at large positive bias voltages.[48] We made use of this fact and measured FERs at different areas of the IPr-NHC/Cu_xO/Cu(111) surface after a 470 K heating treatment performed for 1 min. Figure 4a shows the two main regions, A and B. dI/dV curves taken at large bias voltages on both areas show two different sets of characteristic peaks: A areas present a set of FERs, which corresponds to Cu(111), while the set of FERs on the B areas correspond to Cu_xO.[48] In particular, the dI/dV curves in Figure 4b were taken at the location marked with blue and red dots in Figure 4a. The identification of the chemical nature of A (metallic Cu(111)) and B (Cu_xO/Cu(111)) regions allows for the quantification of the relative amount of metallic areas, which results to be ca. 40% of the surface. Therefore, we can conclude that the Cu_xO species were to a certain extent reduced during the 470 K annealing step.

The same procedure was applied after the 520 K annealing step carried out for 1 min. Figure 4c shows the spots where the dI/dV curves in Figure 4d were taken. In this case, the whole surface shows the same set of FERs, which corresponds to Cu(111).[48] Only a shift in energy is observed on the disordered aggregates. The first peak at 4.4 eV shifts 300 meV, and the rest of the resonances present a shift of ca. 160

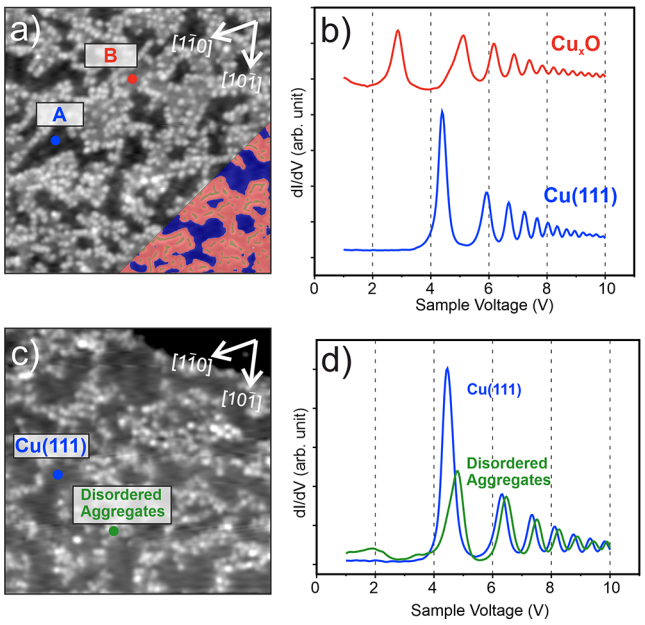

Figure 4. Thermal reduction of the Cu_xO overlayer studied by STM and STS. (a) After 470 K annealing for 1 min. 50 nm × 50 nm, V_s = 1.00 V, I_t = 20 pA. Inset: Cu(111) (blue), Cu_xO (red), and molecules (green) are highlighted. (b) dI/dV acquired on the blue and red dots from (a), exhibiting FERs corresponding to Cu(111) (blue) and Cu_xO (red). (c) After 520 K annealing for 1 min. 50 nm × 50 nm, V_s = −1.5 V, I_t = 120 pA. (d) dI/dV acquired on the blue and green spots in (c), both exhibiting FERs corresponding to metallic Cu(111). A shift in energy is observed on the disordered aggregates.

meV. The different physical origin of the first peak is responsible for the larger energy shift.[48] No areas showing FERs related to Cu_xO were found on the whole surface, suggesting that the Cu_xO layer is completely reduced after the 520 K annealing treatment.

In order to support the findings obtained by STS, additional XPS measurements were carried out. In particular, the as-prepared IPr-NHC/Cu_xO/Cu(111) surface was consecutively heated at different temperatures and characterized by XPS after each annealing treatment. Figure 5 shows the evolution of the N 1s, C 1s, and O 1s peaks. Further analysis of the as-prepared surface was addressed previously by the authors.[49] The intensity of the N 1s peak decreases after heating at 470 K and is barely recognizable after the 520 K annealing step (Figure 5a), which may be related to partial desorption of the IPr-NHC molecules. Interestingly, the intensity of the C 1s peak decreases after heating at 470 K and remains almost constant after treatment at higher temperatures (Figure 5b). Furthermore, a shift in energy of the peak is observed after the annealing at 520 K. This result may be related to the formation of the disordered aggregates discussed above and supports the thermal stability observed in the STM measurements (Figure S3). The dramatic decrease in intensity of the O 1s peak after heating at 470 and 520 K shown in Figure 5c supports the reduction process of the Cu_xO layer discussed in Figure 4. Thermal treatment at higher temperatures does not lead to relevant changes of the O 1s spectra, indicating that, similar to the explanation for the behavior of the C 1s peak, a part of the oxygen atoms may be incorporated into the aggregates.

As a first attempt to model the decomposition of the oxide overlayer by means of DFT calculations, we simulated the creation of an oxygen vacancy in the cuprite overlayer by

https://doi.org/10.1021/acs.jpcc.2c04257
J. Phys. Chem. C 2022, 126, 17528−17535

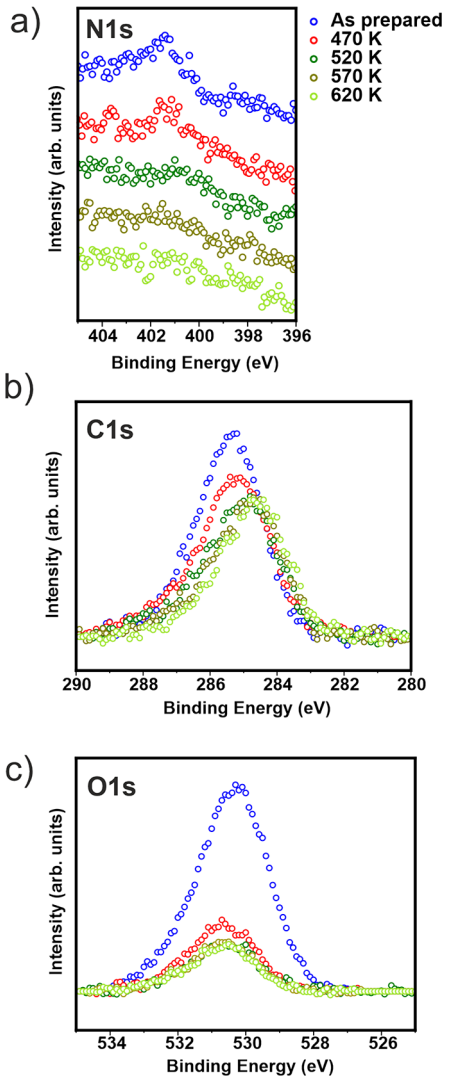

Figure 5. XPS spectra recorded on the as-prepared IPr-NHC/Cu_xO/Cu(111) surface and after successive 1 min-annealing steps (470, 520, 570, and 620 K). (a) N 1s spectra, (b) C 1s spectra, and (c) O 1s spectra. In (b) and (c), a Shirley background has been subtracted.[50]

removing an O atom from the structure shown in Figure 1e,f and comparing the thermodynamic stability of the defective structure with respect to the pristine surface and half an oxygen molecule. The O removal has a cost of 1.10 eV. This value is remarkably small compared to what is normally observed for any bulk oxide but not unusual for metal−supported oxide thin films where a comparable formation energy (1.3 eV) was reported for FeO_2 trilayers supported on Pt(111), for instance.[51] If one considers the entropic contribution of oxygen at standard pressure and finite temperature, the free energy cost is 0.59 eV at T = 470 K and 0.54 eV at T = 520 K. In the absence of any ligand, the process becomes spontaneous only at temperatures above 1000 K, in agreement with the experiments reported by Kirsch and Ekerdt.[33] In this respect, it is important to remember that similar Cu_xO/Cu surfaces like the one studied in the present work can withstand a thermal treatment above 700 K in the absence of ligands.[31]

At this point, it is possible to carry out a discussion of the processes taking place in the present study. In the as-prepared surface, the IPr-NHC ligands bind strongly on the Cu_xO overlayer. After annealing at 470 K for 1 min, the Cu_xO layer gets partially reduced, leading to ca. 40% of metallic Cu(111) areas. Interestingly, IPr-NHC ligands adsorb preferentially on the Cu_xO islands, specially at the edges, in such a way that the metallic areas remain empty. The DFT simulations fully support this evidence, if one looks at the adsorption energy of IPr-NHC in the structures shown in Figure 6a−c (Table S1).

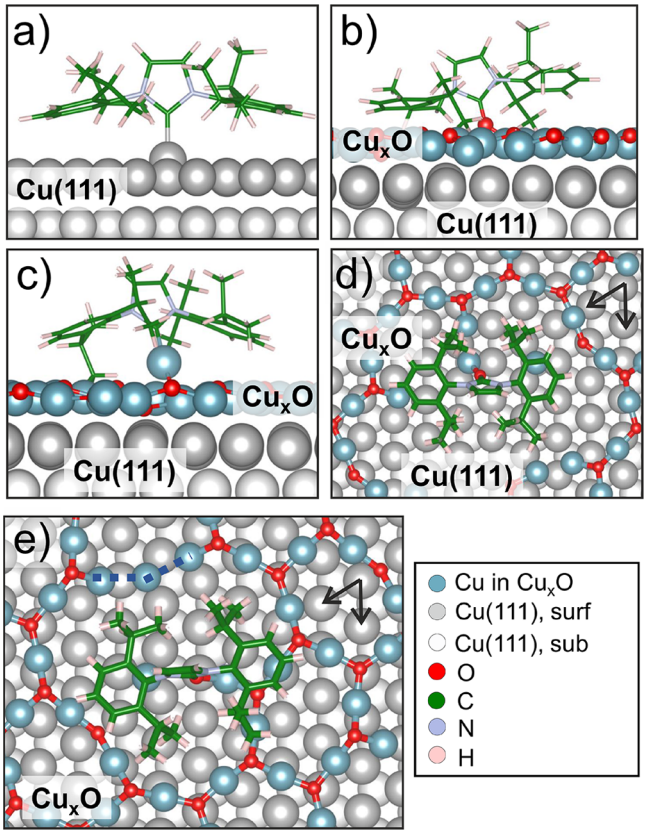

Figure 6. DFT model structures for IPr-NHC adsorbed on (a) Cu(111) (side view); (b) Cu_xO/Cu(111), cyclic urea (side view); (c) Cu_xO/Cu(111), ballbot (side view); (d) border region of Cu_xO/Cu(111), cyclic urea (top view); (e) oxygen-deficient Cu_xO/Cu(111), cyclic urea (top view, the dashed blue line highlights the closest Cu atoms in the overlayer). Cu from Cu(111) (gray), Cu from the Cu_xO/Cu(111) overlayer (metallic blue), O (red), C (green), N (light violet), and H (light pink). Unit cell vectors of Cu(111) are indicated (black arrows).

On metallic Cu(111) (Figure 6a), D_e is as large as −3.68 eV. On oxidized Cu_xO/Cu, various structures were considered (featuring a ligand bound via the carbene end on all possible surface species as well as a physisorbed ligand molecule) and two more stable configurations were identified: in the most stable one (Figure 6b, D_e = −5.01 eV), the NHC ring is bound to an oxygen of the Cu_xO overlayer, while in the other it binds to a Cu ion (Figure 6c, D_e = −3.85 eV). It is thus clear that, if enough thermal energy is provided, the IPr-NHC molecules will diffuse to the oxidized surface regions. In addition to this, we created a surface model displaying a noncontinuous Cu_xO overlayer (Figure 6d) and placed a molecule bound in a carbene-to-oxygen mode: the adsorption energy, however, is −4.90 eV, even slightly smaller compared to the fully oxidized surface. The thermodynamic stability of the molecules adsorbed on the oxidized surface or at the edge looks almost the same, but the edge regions may act as trapping sites when the molecules migrate from the reduced region to the oxidized

https://doi.org/10.1021/acs.jpcc.2c04257
J. Phys. Chem. C 2022, 126, 17528−17535

one during the annealing, which may explain the high concentration of ligands adsorbed in the border region. After the 520 K annealing step, no oxide areas were identified by means of STS, suggesting a full reduction of the Cu_xO overlayer. The disordered aggregates could be related to a possible reaction of the IPr-NHC ligands with Cu_xO at high temperatures. They are remarkably stable, presenting almost no changes in STM images up to 570 K (Figure S3), and may be related to the presence of the C 1s and O 1s signals in XPS after thermal treatment at higher temperatures.

The temperatures reported in this study for the reduction of the Cu_xO overlayer also represent a remarkable result: they are much lower than those for the reduction of Cu_xO in the absence of additional agents.[32,33] The IPr-NHC molecules can thus be considered as promoters of this process. Although the full decomposition process has not been simulated, some further relevant information is provided by DFT calculations. In particular, starting from the structure reported in Figure 6b, we simulated the removal of an oxygen atom in proximity to the adsorbed IPr-NHC molecule, but we obtained the same cost for the defect creation as in the absence of the ligand. We thus cannot assess any direct catalytic role of the ligand in the thermal reduction. However, one should consider that the IPr-NHC adsorption is strongly exothermic, and the amount of energy released on the Cu_xO support upon adsorption is considerable as compared to the cost of an oxygen vacancy creation (1.1 eV). It is also worth noting that the creation of a vacancy in the proximity of a ligand adsorption site leaves the surrounding Cu atoms undercoordinated, promoting a rearrangement where the copper adatoms tend to form clusters at a reciprocal distance of 2.56 Å (blue dashed line in Figure 6e), a value similar to the Cu−Cu equilibrium distance in bulk copper. The role of the ligands may thus be primarily to break the local atomic ordering in the Cu_xO overlayer, promoting the segregation of copper.

CONCLUSIONS

IPr-NHC ligands promote the reduction of an oxidized Cu(111) surface upon heating at moderate temperatures, leading to the appearance of metallic areas. The crucial role of the ligands in this process seems to rely on the displacement of O atoms, which induces the reaggregation of Cu atoms. The local chemical identification of metallic and oxide areas was carried out through the measurements of the FERs by STS. The reduction of the Cu_xO layer is further supported by XPS. The acquisition of the STS curves in the field emission regime thus represents a powerful approach to study different oxidation states appearing in surfaces relevant for heterogeneous catalysis at the nanoscopic level. The present study contributes to a better understanding of reduction mechanisms taking place during thermal catalytic reactions.

ASSOCIATED CONTENT

Supporting Information

The Supporting Information is available free of charge at https://pubs.acs.org/doi/10.1021/acs.jpcc.2c04257.

Synthesis of IPr-CO_2 adduct, copper oxide structures on Cu(111), thermal effects in the range below 470 K, STM height profiles, and adsorption energies of IPr-NHC on copper surfaces (PDF)

AUTHOR INFORMATION

Corresponding Authors

Sergio Tosoni − *Dipartimento di Scienza dei Materiali, Università di Milano-Bicocca, 20125 Milano, Italy;* orcid.org/0000-0001-5700-4086; Email: sergio.tosoni@unimib.it

Markus Heyde − *Department of Interface Science, Fritz-Haber Institute of the Max-Planck Society, 14195 Berlin, Germany;* orcid.org/0000-0002-7049-0485; Email: heyde@fhi-berlin.mpg.de

Frank Glorius − *Westfälische Wilhelms-Universität Münster, Organisch-Chemisches Institut, 48149 Münster, Germany;* orcid.org/0000-0002-0648-956X; Email: glorius@uni-muenster.de

Authors

Juan J. Navarro − *Department of Interface Science, Fritz-Haber Institute of the Max-Planck Society, 14195 Berlin, Germany;* orcid.org/0000-0002-3318-3179

Mowpriya Das − *Westfälische Wilhelms-Universität Münster, Organisch-Chemisches Institut, 48149 Münster, Germany;* orcid.org/0000-0002-3437-0005

Felix Landwehr − *Department of Interface Science, Fritz-Haber Institute of the Max-Planck Society, 14195 Berlin, Germany;* orcid.org/0000-0001-7653-3311

Gianfranco Pacchioni − *Dipartimento di Scienza dei Materiali, Università di Milano-Bicocca, 20125 Milano, Italy;* orcid.org/0000-0002-4749-0751

Beatriz Roldan Cuenya − *Department of Interface Science, Fritz-Haber Institute of the Max-Planck Society, 14195 Berlin, Germany;* orcid.org/0000-0002-8025-307X

Complete contact information is available at: https://pubs.acs.org/10.1021/acs.jpcc.2c04257

Funding

Open access funded by Max Planck Society.

Notes

The authors declare no competing financial interest.

ACKNOWLEDGMENTS

The generous financial support of the Forschungsgemeinschaft (SFB 858 and SFB 1459) is gratefully acknowledged. J.J.N. thanks the Alexander von Humboldt Foundation for financial support. J.J.N., F.L., and M.H. thank Jared P. Bruce for fruitful discussions and support with the XPS measurements. S.T. and G.P. acknowledge the financial support from the Italian Ministry of University and Research (MIUR) through the PRIN Project 20179337R7. Access to the CINECA supercomputing resources was granted via ISCRAB.

REFERENCES

(1) Wachs, I. E. Recent conceptual advances in the catalysis science of mixed metal oxide catalytic materials. *Catal. Today* **2005**, *100*, 79−94.

(2) Arán-Ais, R. M.; Scholten, F.; Kunze, S.; Rizo, R.; Roldan Cuenya, B. The role of in situ generated morphological motifs and Cu(i) species in C2+ product selectivity during CO2 pulsed electroreduction. *Nat. Energy* **2020**, *5*, 317−325.

(3) Jernigan, G. G.; Somorjai, G. A. Carbon Monoxide Oxidation over Three Different Oxidation States of Copper: Metallic Copper, Copper (I) Oxide, and Copper (II) Oxide - A Surface Science and Kinetic Study. *J. Catal.* **1994**, *147*, 567−577.

(4) Newsome, D. S. The Water-Gas Shift Reaction. *Catal. Rev. - Sci. Eng.* **1980**, *21*, 275−318.
(5) Ovesen, C.; Stoltze, P.; Nørskov, J.; Campbell, C. A kinetic model of the water gas shift reaction. *J. Catal.* **1992**, *134*, 445−468.
(6) Hensley, A. J. R.; Therrien, A. J.; Zhang, R.; Marcinkowski, M. D.; Lucci, F. R.; Sykes, E. C. H.; McEwen, J.-S. CO Adsorption on the "29" CuxO/Cu(111) Surface: An Integrated DFT, STM, and TPD Study. *J. Phys. Chem. C* **2016**, *120*, 25387−25394.
(7) Yang, S.; Prendergast, D.; Neaton, J. B. Tuning Semiconductor Band Edge Energies for Solar Photocatalysis via Surface Ligand Passivation. *Nano Lett.* **2012**, *12*, 383−388.
(8) Zhu, Q.; Murphy, C. J.; Baker, L. R. Opportunities for Electrocatalytic CO2 Reduction Enabled by Surface Ligands. *J. Am. Chem. Soc.* **2022**, *144*, 2829−2840.
(9) Bellotti, P.; Koy, M.; Hopkinson, M. N.; Glorius, F. Recent advances in the chemistry and applications of N-heterocyclic carbenes. *Nat. Rev. Chem.* **2021**, *5*, 711−725.
(10) Crudden, C. M.; Horton, J. H.; Narouz, M. R.; Li, Z.; Smith, C. A.; Munro, K.; Baddeley, C. J.; Larrea, C. R.; Drevniok, B.; Thanabalasingam, B.; et al. Simple direct formation of self-assembled N-heterocyclic carbene monolayers on gold and their application in biosensing. *Nat. Commun.* **2016**, *7*, 12654.
(11) Lv, A.; Freitag, M.; Chepiga, K. M.; Schäfer, A. H.; Glorius, F.; Chi, L. N-Heterocyclic-Carbene-Treated Gold Surfaces in Pentacene Organic Field-Effect Transistors: Improved Stability and Contact at the Interface. *Angew. Chem., Int. Ed.* **2018**, *57*, 4792−4796.
(12) MacLeod, M. J.; Goodman, A. J.; Ye, H.-Z.; Nguyen, H. V.-T.; Voorhis, T. V.; Johnson, J. A. Robust gold nanorods stabilized by bidentate N-heterocyclic-carbene−thiolate ligands. *Nat. Chem.* **2019**, *11*, 57−63.
(13) Doud, E. A.; Inkpen, M. S.; Lovat, G.; Montes, E.; Paley, D. W.; Steigerwald, M. L.; Vázquez, H.; Venkataraman, L.; Roy, X. In Situ Formation of N-Heterocyclic Carbene-Bound Single-Molecule Junctions. *J. Am. Chem. Soc.* **2018**, *140*, 8944−8949.
(14) Nguyen, D. T.; Freitag, M.; Körsgen, M.; Lamping, S.; Rühling, A.; Schäfer, A. H.; Siekman, M. H.; Arlinghaus, H. F.; van der Wiel, W. G.; Glorius, F.; et al. Versatile Micropatterns of N-Heterocyclic Carbenes on Gold Surfaces: Increased Thermal and Pattern Stability with Enhanced Conductivity. *Angew. Chem., Int. Ed.* **2018**, *57*, 11465−11469.
(15) Ren, J.; Freitag, M.; Schwermann, C.; Bakker, A.; Amirjalayer, S.; Rühling, A.; Gao, H.-Y.; Doltsinis, N. L.; Glorius, F.; Fuchs, H. A Unidirectional Surface-Anchored N-Heterocyclic Carbene Rotor. *Nano Lett.* **2020**, *20*, 5922−5928.
(16) Singh, I.; Lee, D. S.; Huang, S.; Bhattacharjee, H.; Xu, W.; McLeod, J. F.; Crudden, C. M.; She, Z. N-Heterocyclic carbenes meet toll-like receptors. *Chem. Commun.* **2021**, *57*, 8421−8424.
(17) Ranganath, K. V. S.; Kloesges, J.; Schäfer, A. H.; Glorius, F. Asymmetric Nanocatalysis: N-Heterocyclic Carbenes as Chiral Modifiers of Fe3O4/Pd nanoparticles. *Angew. Chem., Int. Ed.* **2010**, *49*, 7786−7789.
(18) Zhukhovitskiy, A. V.; MacLeod, M. J.; Johnson, J. A. Carbene Ligands in Surface Chemistry: From Stabilization of Discrete Elemental Allotropes to Modification of Nanoscale and Bulk Substrates. *Chem. Rev.* **2015**, *115*, 11503−11532.
(19) Ernst, J. B.; Muratsugu, S.; Wang, F.; Tada, M.; Glorius, F. Tunable Heterogeneous Catalysis: N-Heterocyclic Carbenes as Ligands for Supported Heterogeneous Ru/K-Al2O3 Catalysts To Tune Reactivity and Selectivity. *J. Am. Chem. Soc.* **2016**, *138*, 10718−10721.
(20) Ernst, J. B.; Schwermann, C.; Yokota, G.-i.; Tada, M.; Muratsugu, S.; Doltsinis, N. L.; Glorius, F. Molecular Adsorbates Switch on Heterogeneous Catalysis: Induction of Reactivity by N-Heterocyclic Carbenes. *J. Am. Chem. Soc.* **2017**, *139*, 9144−9147.
(21) Cao, Z.; Derrick, J. S.; Xu, J.; Gao, R.; Gong, M.; Nichols, E. M.; Smith, P. T.; Liu, X.; Wen, X.; Copéret, C.; et al. Chelating N-Heterocyclic Carbene Ligands Enable Tuning of Electrocatalytic CO2 Reduction to Formate and Carbon Monoxide: Surface Organometallic Chemistry. *Angew. Chem., Int. Ed.* **2018**, *57*, 4981−4985.
(22) Smith, C. A.; Narouz, M. R.; Lummis, P. A.; Singh, I.; Nazemi, A.; Li, C.-H.; Crudden, C. M. N-Heterocyclic Carbenes in Materials Chemistry. *Chem. Rev.* **2019**, *119*, 4986−5056.
(23) Koy, M.; Bellotti, P.; Das, M.; Glorius, F. N-Heterocyclic carbenes as tunable ligands for catalytic metal surfaces. *Nat. Catal.* **2021**, *4*, 352−363.
(24) Kaeffer, N.; Mance, D.; Copéret, C. N-Heterocyclic Carbene Coordination to Surface Copper Sites in Selective Semihydrogenation Catalysts from Solid-State NMR Spectroscopy. *Angew. Chem., Int. Ed.* **2020**, *59*, 19999−20007.
(25) Tappan, B. A.; Chen, K.; Lu, H.; Sharada, S. M.; Brutchey, R. L. Synthesis and Electrocatalytic HER Studies of Carbene-Ligated Cu3-xP Nanocrystals. *ACS Appl. Mater. Interfaces* **2020**, *12*, 16394−16401.
(26) Jiang, L.; Zhang, B.; Médard, G.; Seitsonen, A. P.; Haag, F.; Allegretti, F.; Reichert, J.; Kuster, B.; Barth, J. V.; Papageorgiou, A. C. N-Heterocyclic carbenes on close-packed coinage metal surfaces: bis-carbene metal adatom bonding scheme of monolayer films on Au, Ag and Cu. *Chem. Sci.* **2017**, *8*, 8301−8308.
(27) Veinot, A. J.; Al-Rashed, A.; Padmos, J. D.; Singh, I.; Lee, D. S.; Narouz, M. R.; Lummis, P. A.; Baddeley, C. J.; Crudden, C. M.; Horton, J. H. N-Heterocyclic Carbenes Reduce and Functionalize Copper Oxide Surfaces in One Pot. *Chem.—Eur. J.* **2020**, *26*, 11431−11434.
(28) Larrea, C. R.; Baddeley, C. J.; Narouz, M. R.; Mosey, N. J.; Horton, J. H.; Crudden, C. M. N-Heterocyclic Carbene Self-assembled Monolayers on Copper and Gold: Dramatic Effect of Wingtip Groups on Binding, Orientation and Assembly. *ChemPhysChem* **2017**, *18*, 3536−3539.
(29) Ren, J.; Freitag, M.; Gao, Y.; Bellotti, P.; Das, M.; Schulze Lammers, B.; Mönig, H.; Zhang, Y.; Daniliuc, C. G.; Du, S.; et al. Reversible Self-Assembly of an N-Heterocyclic Carbene on Metal Surfaces. *Angew. Chem., Int. Ed.* **2022**, *61*, No. e202115104.
(30) Navarro, J. J.; Das, M.; Tosoni, S.; Landwehr, F.; Koy, M.; Heyde, M.; Pacchioni, G.; Glorius, F.; Cuenya, B. R. Growth of N-Heterocyclic Carbene Assemblies on Cu(100) and Cu(111): from Single Molecules to Magic-Number Islands. *Angew. Chem., Int. Ed.* **2022**, *61*, No. e202202127.
(31) Matsumoto, T.; Bennett, R.; Stone, P.; Yamada, T.; Domen, K.; Bowker, M. Scanning tunneling microscopy studies of oxygen adsorption on Cu(111). *Surf. Sci.* **2001**, *471*, 225−245.
(32) Li, J.; Vizkelethy, G.; Revesz, P.; Mayer, J. W.; Tu, K. N. Oxidation and reduction of copper oxide thin films. *J. Appl. Phys.* **1991**, *69*, 1020−1029.
(33) Kirsch, P. D.; Ekerdt, J. G. Chemical and thermal reduction of thin films of copper (II) oxide and copper (I) oxide. *J. Appl. Phys.* **2001**, *90*, 4256−4264.
(34) Van Ausdall, B. R.; Glass, J. L.; Wiggins, K. M.; Aarif, A. M.; Louie, J. A Systematic Investigation of Factors Influencing the Decarboxylation of Imidazolium Carboxylates. *J. Org. Chem.* **2009**, *74*, 7935−7942.
(35) Wang, G.; Rühling, A.; Amirjalayer, S.; Knor, M.; Ernst, J. B.; Richter, C.; Gao, H.-J.; Timmer, A.; Gao, H.-Y.; Doltsinis, N. L.; et al. Ballbot-type motion of N-heterocyclic carbenes on gold surfaces. *Nat. Chem.* **2017**, *9*, 152−156.
(36) Kresse, G.; Furthmüller, J. Efficiency of ab-initio total energy calculations for metals and semiconductors using a plane-wave basis set. *Comput. Mater. Sci.* **1996**, *6*, 15−50.
(37) Kresse, G.; Furthmüller, J. Efficient iterative schemes for ab initio total-energy calculations using a plane-wave basis set. *Phys. Rev. B* **1996**, *54*, 11169−11186.
(38) Blöchl, P. E. Projector augmented-wave method. *Phys. Rev. B* **1994**, *50*, 17953−17979.
(39) Kresse, G.; Joubert, D. From ultrasoft pseudopotentials to the projector augmented-wave method. *Phys. Rev. B* **1999**, *59*, 1758−1775.
(40) Perdew, J. P.; Burke, K.; Ernzerhof, M. Generalized Gradient Approximation Made Simple. *Phys. Rev. Lett.* **1996**, *77*, 3865−3868.

(41) Grimme, S. Semiempirical GGA-type density functional constructed with a long-range dispersion correction. *J. Comput. Chem.* **2006**, *27*, 1787−1799.
(42) Tosoni, S.; Sauer, J. Accurate quantum chemical energies for the interaction of hydrocarbons with oxide surfaces: CH4/MgO(001). *Phys. Chem. Chem. Phys.* **2010**, *12*, 14330−14340.
(43) Therrien, A. J.; Zhang, R.; Lucci, F. R.; Marcinkowski, M. D.; Hensley, A.; McEwen, J.-S.; Sykes, E. C. H. Structurally Accurate Model for the "29"-Structure of CuxO/Cu(111): A DFT and STM Study. *J. Phys. Chem. C* **2016**, *120*, 10879−10886.
(44) Gattinoni, C.; Michaelides, A. Atomistic details of oxide surfaces and surface oxidation: the example of copper and its oxides. *Surf. Sci. Rep.* **2015**, *70*, 424−447.
(45) Jensen, F.; Besenbacher, F.; Stensgaard, I. Two new oxygen induced reconstructions on Cu(111). *Surf. Sci.* **1992**, *269*−*270*, 400−404.
(46) Huang, M.; Zhong, Y.; Lu, S.; Guo, Q.; Yu, Y. Antimony allotropes fabricated on oxide layer of Cu(111). *Thin Solid Films* **2021**, *727*, 138669.
(47) Wiame, F.; Maurice, V.; Marcus, P. Initial stages of oxidation of Cu(111). *Surf. Sci.* **2007**, *601*, 1193−1204.
(48) Navarro, J. J.; Tosoni, S.; Bruce, J. P.; Chaves, L.; Heyde, M.; Pacchioni, G.; Cuenya, B. R. Structure of a Silica Thin Film on Oxidized Cu(111): Conservation of the Honeycomb Lattice and Role of the Interlayer. *J. Phys. Chem. C* **2020**, *124*, 20942−20949.
(49) Navarro, J. J.; Das, M.; Tosoni, S.; Landwehr, F.; Bruce, J. P.; Heyde, M.; Pacchioni, G.; Glorius, F.; Cuenya, B. R. Covalent Adsorption of N-Heterocyclic Carbenes on a Copper Oxide Surface. *J. Am. Chem. Soc.* **2022**, *144*, 16267−16271.
(50) Shirley, D. A. High-Resolution X-Ray Photoemission Spectrum of the Valence Bands of Gold. *Phys. Rev. B* **1972**, *5*, 4709−4714.
(51) Sun, Y.-N.; Giordano, L.; Goniakowski, J.; Lewandowski, M.; Qin, Z.-H.; Noguera, C.; Shaikhutdinov, S.; Pacchioni, G.; Freund, H.-J. The Interplay between Structure and CO Oxidation Catalysis on Metal-Supported Ultrathin Oxide Films. *Angew. Chem., Int. Ed.* **2010**, *49*, 4418−4421.

https://doi.org/10.1021/acs.jpcc.2c04257
J. Phys. Chem. C 2022, 126, 17528−17535